The Journal of Green Energy and Environmental Engineering

Research Paper

Preparation and Properties of Cellulose Nanocrystal Based Structurally Colored Radiative Cooling Composite Films

Mikhail Volkov[1,*]

[1] Department of Mechanical Engineering, Thiagarajar College of Engineering, Madurai University, Madurai 625 015, Tamilnadu, India

*Corresponding author: Volkov@moore.sc.edu

Abstract. Radiative cooling is a green, low-carbon, and sustainable cooling strategy that lowers its own temperature by emitting heat into outer space. Most radiative cooling materials exhibit monotonous color appearances, mostly white or transparent, and the addition of traditional colorants causes heat absorption, thereby reducing radiative cooling performance. In this study, cellulose nanocrystal/polyethylene glycol (CNC/PEG) composite radiative cooling films with tunable structural colors were prepared via a self-assembly method. These composite films were subsequently combined with porous cellulose acetate (CA) films to obtain structurally colored radiative cooling bilayer composite films. The results indicate that the CNC/PEG composite films exhibit vivid structural colors with distinct birefringence phenomena. As the PEG content increases, the pitch of the composite film structure enlarges, and the color shifts from blue-green to red. The CNC/PEG structural color composite film achieves a maximum reflectance of up to 68.5% in the visible light band and an emissivity of up to 93% in the atmospheric window band, demonstrating an ambient cooling effect of approximately 3.4 °C. The CNC/PEG-CA bilayer composite film attains a maximum reflectance of up to 91.8% in the visible light band and an emissivity of up to 32.2% in the atmospheric window band. Compared with the single-layer composite film, the bilayer composite film exhibits superior cooling performance, with a temperature difference of approximately 14.3 °C relative to the ambient temperature. In outdoor tests, the composite film achieves a cooling effect of approximately 2 °C, while the bilayer composite film achieves a cooling effect of approximately 6 °C compared to the ambient temperature.

Keywords: *Radiative cooling; Structural color; Cellulose nanocrystals; Chiral nematic structure; Bilayer composite film*

Received on 02 March 2023, Accepted on 28 May 2023, Published on 15 July 2023

1 Introduction

Currently, the negative impacts of global warming have severely affected human production and daily life[1-2]. Excessive energy consumption and scarcity further exacerbate environmental issues, making thermal management a primary challenge[3-5]. The Earth's surface temperature is approximately 300 K, while the average temperature of outer space is 3 K[6-7]. According to the second law of thermodynamics, heat from terrestrial objects can be radiated into outer space due to this temperature gradient. Therefore, radiative cooling technology enables terrestrial objects to radiate heat into outer space through the "atmospheric window" band (8–13 μm)[8-10], thereby achieving self-cooling.

Although radiative cooling materials demonstrate significant potential in energy conservation and environmental protection[10], existing materials are predominantly white or silvery-white with monotonous appearances, resulting in low utilization rates. Dyes can alter the surface color of materials; however, their visible coloration absorbs heat and additionally absorbs heat within the near-infrared band[11-12], diminishing the

material's inherent cooling efficiency. To date, the primary strategy to overcome this issue is to enhance reflectance in the visible region and emissivity in the "atmospheric window" band (8–13 μm)[13-16]. To avoid heat absorption by dyes, structurally colored radiative cooling materials have garnered widespread attention[17-18]. While structurally colored radiative cooling materials can be fabricated using silica opals, this approach fails to achieve sub-ambient cooling[19]and involves complex, stringent production processes, hindering large-scale manufacturing and application.

Cellulose nanocrystals (CNCs) are rigid rod-like particles with lengths ranging from tens to hundreds of nanometers and diameters reaching tens of nanometers[20], characterized by high crystallinity and biodegradability. CNCs can be extracted from renewable resources such as cotton, wood, and pulp, offering advantages including low cost, environmental friendliness, and sustainability[21-23]. CNCs spontaneously organize into a chiral nematic liquid crystalline phase in water, and this ordered structure is retained during the drying process, ultimately yielding CNC films with a chiral nematic structure[24]. The helical arrangement of birefringent CNC nanorods within the film creates periodic variations in the refractive index of the nanostructure, leading to strong reflection of visible light[25]. Consequently, the modulation of structural color is intrinsically linked to the periodicity of the helical structure.

Current research endeavors focus on fabricating cellulose-based radiative cooling materials with richer coloration. Shanker et al.[26]prepared a structurally colored radiative cooling device by self-assembling CNCs into structural color films bonded to silicon wafer substrates. By controlling the CNC/glycerol (GLU) mass ratio, composite films with colors shifting from blue-violet to red were obtained. These structural color composite films exhibited low absorptance in the solar spectrum and high emissivity in the "atmospheric window," with green and red samples achieving cooling effects of approximately 9 °C and blue-violet samples achieving approximately 6 °C. This provides a foundational basis for preparing cellulose-based structural color radiative cooling films.

In this study, CNCs were composited with polyethylene glycol (PEG), and structurally colored films with high solar reflectance and high emissivity in the "atmospheric window" band were fabricated via a self-assembly method. By controlling the mass ratio of CNC to PEG, the structural color of the composite films was modulated to achieve thermal emissivity control across different wavelengths. The effects of varying PEG additions on the structure, optical properties, and cooling performance of the CNC composite structural color films were investigated. Furthermore, the composite structural color films were laminated onto cellulose acetate filter membranes to prepare bilayer composite films, and their radiative cooling effects were further explored.

2 Experimental Materials and Methods

2.1 Raw Materials

Cellulose acetate: Shanghai Xingya Purification Material Factory; Concentrated sulfuric acid (H_2SO_4): Analytical reagent, Aladdin Century Co., Ltd.; Polyethylene glycol 400: Analytical reagent, Tianjin Kemiou Chemical Reagent Co., Ltd.

2.2 Experimental Procedure

Preparation of CNC: CNC was prepared via acid hydrolysis. Specifically, 200 mL of 64% sulfuric acid solution was slowly poured into 25 g of sulfate-bleached softwood pulp under stirring at 45 °C in a water bath for 1 h. The hydrolysis reaction was terminated by adding a large volume of distilled water. After standing for 2–3 days, the supernatant was removed. The precipitate was subjected to multiple centrifugal washing cycles using a high-speed centrifuge (CT14D, Shanghai Tianmei Instrument Co., Ltd.) with deionized water. The resulting CNC suspension was dialyzed against deionized water until neutral pH was achieved. Finally, the CNC suspension was concentrated to 3 wt% and stored refrigerated for future use.

Preparation of CNC/PEG Composite Films: 5.0 g of polyethylene glycol was dissolved in 45 g of ultrapure water and stirred at room temperature for 1 h to obtain a 10 wt% PEG solution. 3.0 g of the 3 wt% CNC suspension was ultrasonicated for 5 min. Four aliquots of the CNC suspension were separately mixed with 0.1000 g, 0.2250

g, 0.3857 g, and 0.6000 g of PEG solution. The mixtures were stirred thoroughly for 2 h and then poured into circular containers to undergo slow evaporation at room temperature for 2–3 days, yielding CNC/PEG composite structural color films with PEG concentrations of 10 wt%, 20 wt%, 30 wt%, and 40 wt%, respectively. The composite films were named according to the type and content of polymers: CNC/PEG-10%, CNC/PEG-20%, CNC/PEG-30%, and CNC/PEG-40% (Table 1).

Table 1 Naming of cellulose nanocrystal/polyethylene glycol (CNC/PEG) composite radiative cooling films and CNC/PEG-cellulose acetate (CA) structurally colored radiative cooling bilayer composite films

Sample	Mass fraction of CNC/wt%	Mass fraction of PEG/wt%	CA
CNC/PEG-10%	3	10	—
CNC/PEG-20%	3	20	—
CNC/PEG-30%	3	30	—
CNC/PEG-40%	3	40	—
CNC/PEG-10%-CA	3	10	0.0740 g
CNC/PEG-20%-CA	3	20	0.0740 g
CNC/PEG-30%-CA	3	30	0.0740 g
CNC/PEG-40%-CA	3	40	0.0740 g

Preparation of Bilayer Composite Films: The composite structural color films with different mass ratios were adhered to cellulose acetate membranes using double-sided tape. The tape was placed at the edges of the CA membrane for fixation and did not interfere with the bilayer composite structural color film structure. The bilayer composite structural color films were named CNC/PEG-10%-CA, CNC/PEG-20%-CA, CNC/PEG-30%-CA, and CNC/PEG-40%-CA (Table 1).

2.3 Testing and Characterization

2.3.1 Performance Analysis of CNC/PEG Composite Films

The Zeta potential and particle size of CNC were measured using a Malvern Zetasizer Nano ZS90. The liquid crystalline properties of the composite film samples were observed using a polarizing optical microscope (POM, XPF-550C, Shanghai CaiKang Optical Instrument Co., Ltd.). Reflection spectra of the films were acquired using a reflection spectrometer (UV-vis, HR4000 CG-NIR, Ocean Insight) in the visible region. For cross-sectional morphology observation, composite films were cryo-fractured in liquid nitrogen, mounted on stubs using double-sided conductive adhesive, and sputter-coated with gold for 60 s prior to scanning electron microscopy (SEM, JSM-7500F, JEOL Ltd.). The reflectance changes of samples within the 300–2500 nm wavelength range were detected using a UV-Vis-NIR spectrophotometer equipped with an integrating sphere (PerkinElmer, USA). The absorbance changes of samples within the 2.5–25 μm wavelength range were measured using a Fourier-transform infrared spectrometer (FTIR, Nicolet IS10, Thermo Fisher Scientific, USA). A high-power xenon lamp (CEAuLight HXF300) with a solar spectrum match was employed to simulate sunlight irradiation. A 1 cm × 1 cm × 1 cm cavity was carved into a polystyrene (PS) foam box, and the film or composite film was placed inside the cavity for fixation. The foam box was covered with polyethylene film to eliminate environmental convective heat transfer. A multi-channel thermometer (JINKO, JK804) connected to two K-type thermocouples was used: one thermocouple measured the internal temperature of the cavity beneath the composite film, while the other measured the ambient temperature inside the device covered by the polyethylene film. Notably, the CNC/PEG-40% composite film absorbs ambient moisture during characterization, causing swelling of the chiral structure and altering the pitch, which is detrimental to practical applications. Therefore, SEM, spectroscopic, and radiative cooling performance tests were not conducted on the CNC/PEG-40% composite film.

2.3.2 Performance Analysis of Bilayer Composite Films

Cellulose acetate films were adhered to horizontal stubs using conductive adhesive, sputter-coated with gold for 60 s, and their surface morphologies were observed via SEM. Temperature variations under the same xenon lamp source were monitored using an infrared thermal imager (FLIR E390, FLIR Systems, USA). The aforementioned self-assembled setup was utilized to measure the temperature beneath the bilayer composite films and the ambient temperature inside the entire device covered by polyethylene film. Outdoor cooling performance tests were conducted using a laboratory-built self-assembled apparatus. The indoor testing setup was placed inside a cardboard box wrapped in aluminum foil, positioned atop a foam box. A hygrometer recorded ambient humidity changes during testing.

3 Results and Discussion

3.1 Potential and Particle Size Analysis of Cellulose Nanocrystals

Fig. 1 shows the TEM image, particle size distribution, and Zeta potential curve of CNC. Acid-hydrolyzed CNC exhibits a rod-like morphology with an average particle size of 144.1 nm (Fig. 1(b)). During hydrolysis, numerous negative charges form on the CNC surface, resulting in a Zeta potential as high as –32.2 mV (Fig. 1(c)). These abundant surface negative charges enhance electrostatic repulsion, improving the stability of the CNC suspension and laying the groundwork for subsequent structural color composite film fabrication.

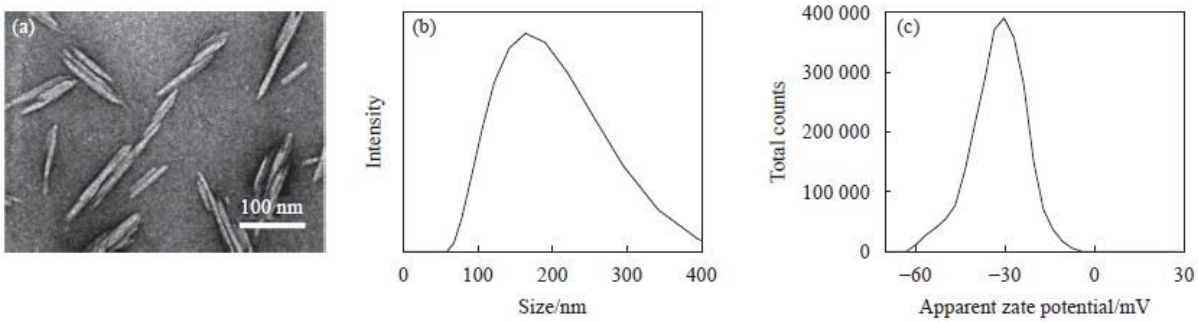

Figure 1 (a) TEM image of CNC; (b) Particle size distribution of CNC; (c) Zeta potential curve of CNC

3.2 Optical Characteristics of Structural Color in CNC Composite Films

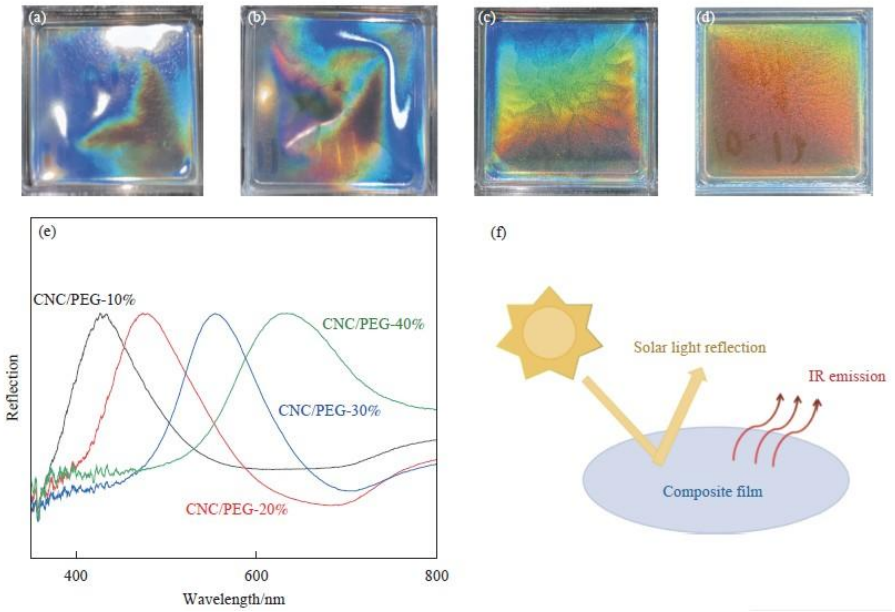

Figure 2 ((a)–(d)) Digital photographs of CNC/PEG-10%, CNC/PEG-20%, CNC/PEG-30%, CNC/PEG-40%;

(e) UV-vis reflection spectra of CNC/PEG; (f) Schematic of composite film radiative cooling

Figs. 2(a)–2(d) present digital photographs of composite films with varying PEG contents. As the PEG content increases, the reflected color of the films exhibits a redshift, gradually shifting from blue-green to red. This redshift phenomenon in the structural color correlates with the PEG content. Analysis of the UV-Vis reflection spectra (Fig. 2(e)) reveals that with increasing PEG content, the four composite films exhibit distinct peaks at 427 nm, 487 nm, 576 nm, and 654 nm, respectively. The highest peak in the reflection spectra redshifts correspondingly with the visual color shift. Fig. 2(f) illustrates that the composite films achieve self-cooling by reflecting visible light and emitting thermal radiation, providing a theoretical basis for subsequent radiative cooling research.

3.3 Microscopic Morphology Analysis of CNC Composite Films

Figs. 3(a)–3(c) display cross-sectional SEM images of composite films with different PEG contents. Since the CNC/PEG-40% film absorbs ambient moisture, causing swelling of the chiral structure and altering the pitch during measurement, SEM analysis was restricted to films with 10–30 wt% PEG.

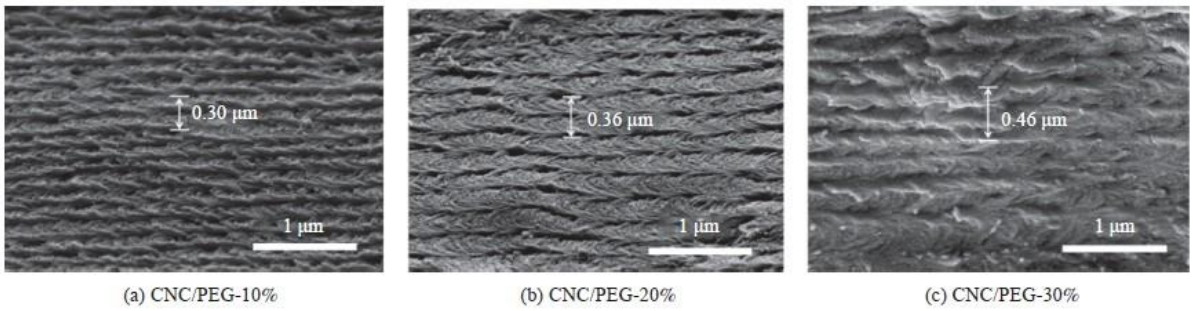

Figure 3 Cross-sectional electron microscope images of composite films with different PEG contents

Pure CNC films exhibit a periodic layered structure. CNCs rotate counterclockwise to form a left-handed chiral nematic helical structure. This left-handed chiral nematic structure reflects left-handed circularly polarized light of specific wavelengths, endowing the composite film with unique iridescence. The incorporation of polymers does not disrupt the inherent chiral nematic structure of CNC. However, with increasing polymer content, the pitch of the CNC chiral nematic structure increases markedly. In Bragg's equation, the pitch (P) of the chiral nematic structure is defined as the interlayer spacing generated by a 360° rotation of CNC rods, visually represented as the spacing between adjacent layers in SEM images. The gradual increase in pitch is primarily attributed to PEG macromolecules penetrating the CNC chiral nematic structure, causing expansion of the pitch Pand consequently the redshift in film color.

3.4 Refraction Phenomena in CNC Composite Films

Fig. 4 presents POM images of composite films with varying PEG contents. Figs. 4(a)–4(d) confirm distinct birefringence in the films. High-magnification POM images (Figs. 4(e)–4(h)) reveal clear fingerprint textures, indicating that CNC/PEG retained its chiral nematic structure during drying and post-film formation. Therefore, moderate PEG addition does not disrupt the chiral nematic structure formed by CNC self-assembly. The fingerprint texture spacing widens progressively with increasing PEG content, measuring 2.05 μm, 2.33 μm, 2.84 μm, and 3.38 μm, respectively, accompanying a color shift from blue-green to bluish-red. PEG occupies the interstitial spaces between CNCs within the chiral nematic structure, leading to an increased pitch Pand consequent redshift. Analysis of POM results confirms that the reflected light from CNC/PEG composite films adheres to Bragg's law:

$$\lambda = nP\cos(\theta) \quad (1)$$

where λ is the reflection wavelength, n is the average refractive index of the film, θis the incident angle, and Pis the interlayer spacing of the chiral nematic structure.

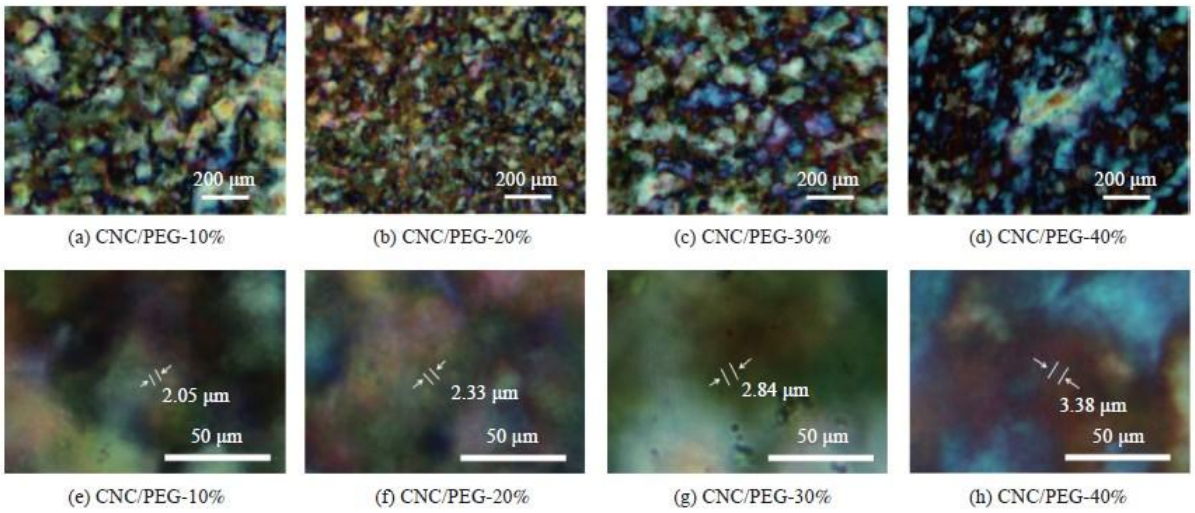

Figure 4 Polarized light microscopy images of composite films with different PEG contents

Since the refractive indices of CNC and PEG are similar (1.41 and 1.44, respectively), the average refractive index (n) can be considered constant. When the incident angle (θ) is fixed, λdepends on the pitch P. The average pitches measured from Figs. 3(a)–3(c) are 0.30 μm, 0.36 μm, and 0.46 μm, respectively. As the average pitch Pincreases, the reflection wavelength λincreases accordingly, proving that PEG addition preserves the chiral nematic structure and birefringence of CNC. Controlling the PEG content effectively modulates the chiral nematic layer spacing, thereby tuning the structural color of the composite films.

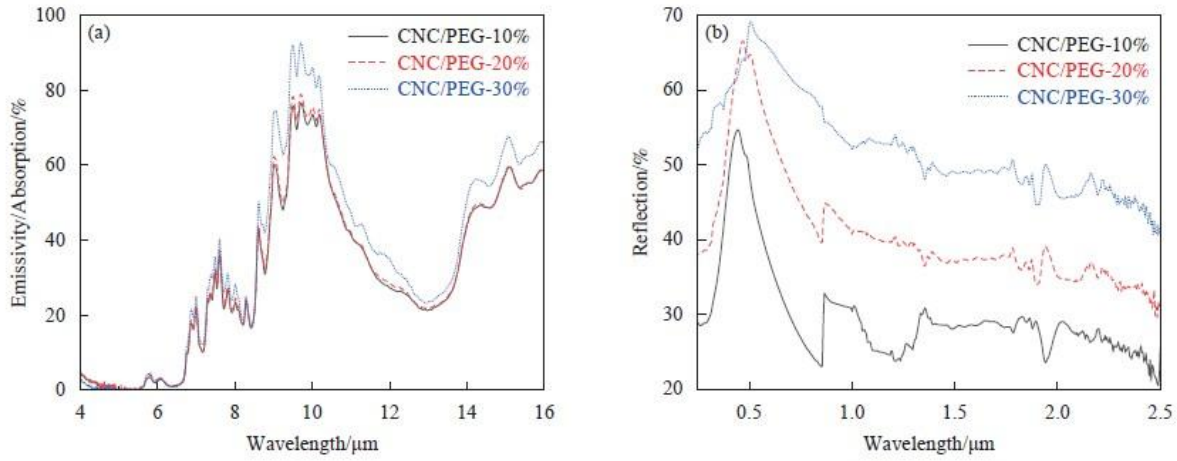

Figure 5 Composite films with different PEG contents: (a) Emissivity profile; (b) Reflectivity profile in the visible light range

3.5 Spectroscopic Analysis of CNC Structural Color Composite Films and Bilayer Composite Films

According to Kirchhoff's law, the emissivity (ε) of a sample equals its absorptance (A). Fig. 5(a) shows that under an indoor humidity of 42%, all samples exhibit high emissivity within the atmospheric window band (8–13 μm). Specifically, the composite film with 30 wt% PEG achieves a maximum emissivity of 93.0%, maximizing infrared heat radiation to the sky. The high emissivity of CNC/PEG composite films stems from intense stretching and bending vibrations of O–H (6.9–7.6 μm), C–O (7.6–9.5 μm), and C–H (11.1–14.3 μm) bonds within the atmospheric window range. Fig. 5(b) presents the solar reflectance curves of composite films with varying PEG contents within the solar spectrum (0.3–2.5 μm). The structural color composite films achieve a maximum reflectance of up to 68.5% in the near-infrared region. Reflectance increases progressively with higher PEG content.

Fig. 6 shows the emissivity curves and visible light reflectance curves of bilayer composite cooling films with different PEG contents. Under the measurement environment with 42% indoor humidity (Fig. 6(a)), the emissivity of the bilayer composite films in the atmospheric window exceeds that of the pure cellulose acetate film. Emissivity rises with increasing PEG content, peaking at 68.0% for the film with 30 wt% PEG. Fig. 6(b) displays the solar reflectance curves of bilayer composite films with varying PEG contents within the 0.3–2.5 μm range. The maximum reflectance in the near-infrared region reaches 91.8%.

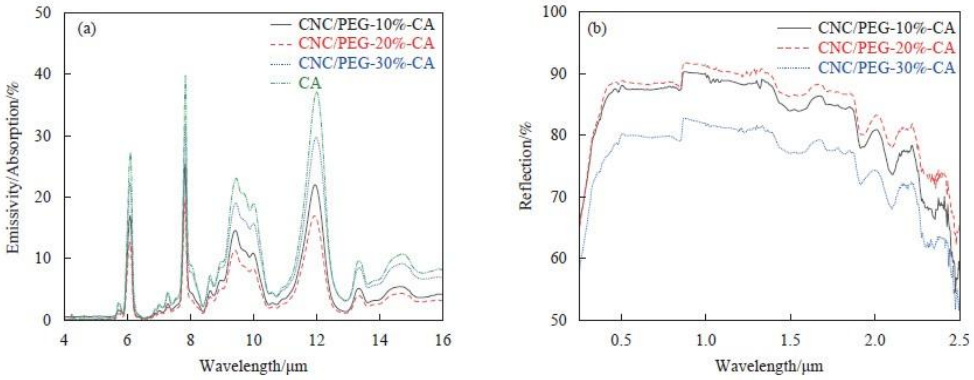

Figure 6 Bilayer composite films with different PEG contents: (a) Emissivity profile; (b) Reflectivity profile in the visible light range

3.6 Radiative Cooling Performance Analysis of CNC Composite Structural Color Films and Bilayer Composite Films

Fig. 7(a) depicts the indoor xenon lamp simulation setup. Irradiation with a 100 mW/cm² high-power xenon lamp simulates sunlight while ensuring uniform light distribution on the sample surface. Fig. 7(b) illustrates the self-assembled temperature measurement device. The polyethylene (PE) film permits light transmission while minimizing convective heat transfer interference with radiative cooling results. Upon turning on the xenon lamp (Figs. 7(c), 7(d)), the internal temperature of the PE-covered device rose rapidly, stabilizing after 5 min. Once thermal equilibrium was approached, the temperature beneath the films was significantly lower than the air temperature inside the PE-covered device. Different structural color CNC/PEG composite films exhibited similar radiative cooling performance, averaging a cooling effect of approximately 3.4 °C.

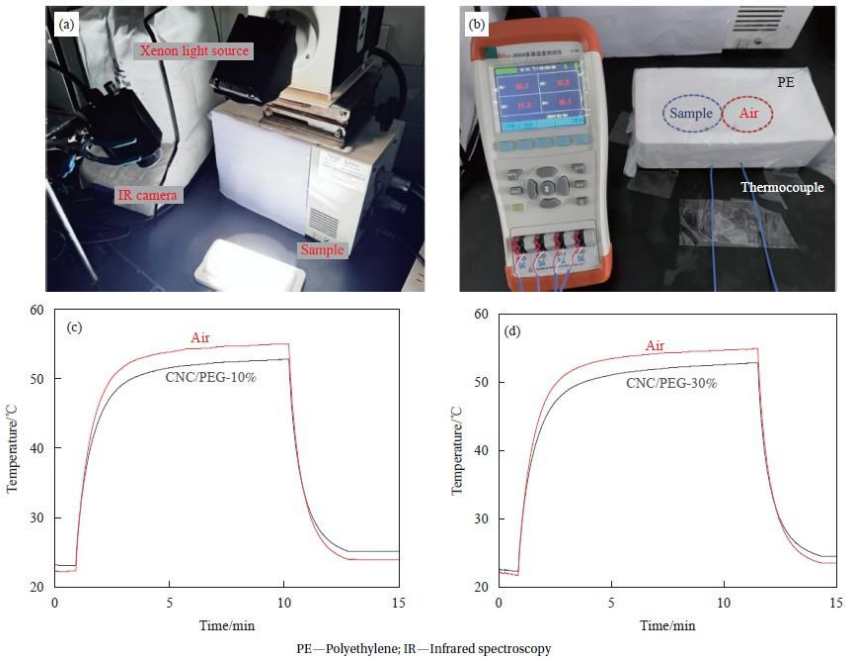

PE—Polyethylene; IR—Infrared spectroscopy

Figure 7 (a) Photos of indoor Xenon lamp simulation device; (b) Self-assembling temperature measuring device; Temperature comparison of CNC/PEG-10% and air (c), CNC/PEG-30% and air (d)

Figs. 8(a)–8(c) present infrared thermograms of cellulose acetate (CA) film, filter paper, and A4 paper under the same light source. After 5 min of xenon lamp irradiation, the CA film exhibited the lowest surface temperature, filter paper was slightly higher, and A4 paper was the highest. SEM imaging of the CA film (Fig. 8(d)) revealed a porous structure capable of effectively reflecting visible light. Fig. 8(e) compares the temperature beneath the CA film against ambient temperature, showing an average temperature reduction of approximately 15 °C. These results confirm the excellent radiative cooling capacity of CA film, making it an optimal substrate for the bilayer composite film.

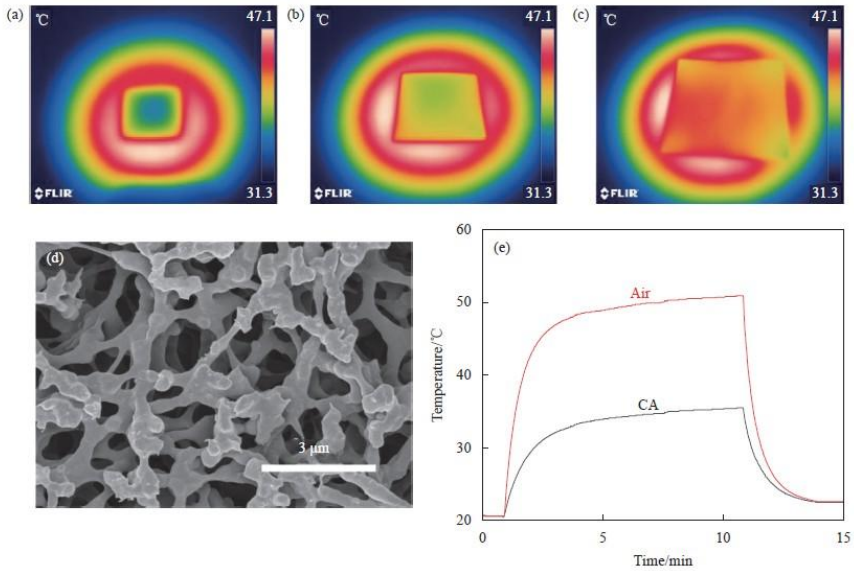

Figure 8 ((a)–(c)) Infrared thermograms of cellulose acetate (CA) film, filter paper and A4 paper; (d) SEM image of CA film surface; (e) Temperature comparison of CA and air

Infrared thermography compared the surface cooling capabilities of CNC/PEG-20%, CNC/PEG-20%-CA, and blue paint-coated CA films under identical illumination duration and intensity (Figs. 9(a)–9(c)). CNC/PEG-20%-CA exhibited the strongest surface cooling, followed by CNC/PEG-20%, while the blue paint-coated CA film performed the worst. Analysis of temperature curves for CNC/PEG-20% and the blue paint-coated CA film (Figs. 9(d), 9(e)) further corroborates the superior cooling performance of the bilayer composite film. The starting temperatures beneath the PE film-covered device and the bilayer composite cooling film were similar (Figs. 9(f), 9(g)). Upon xenon lamp activation, both temperatures rose swiftly, stabilizing after 5 min. At equilibrium, the temperature beneath the bilayer composite cooling film was substantially lower than the internal air temperature. The radiative cooling performance of the bilayer composite film was largely unaffected by PEG content, averaging a cooling effect of approximately 14.3 °C—significantly outperforming the single-layer composite film. Experimental results indicate: CNC/PEG composite films average a cooling of ~3.4 °C; CA film serves as an ideal substrate for bilayer composites; and the bilayer composite cooling film averages a cooling of ~14.3 °C, surpassing the single-layer film.

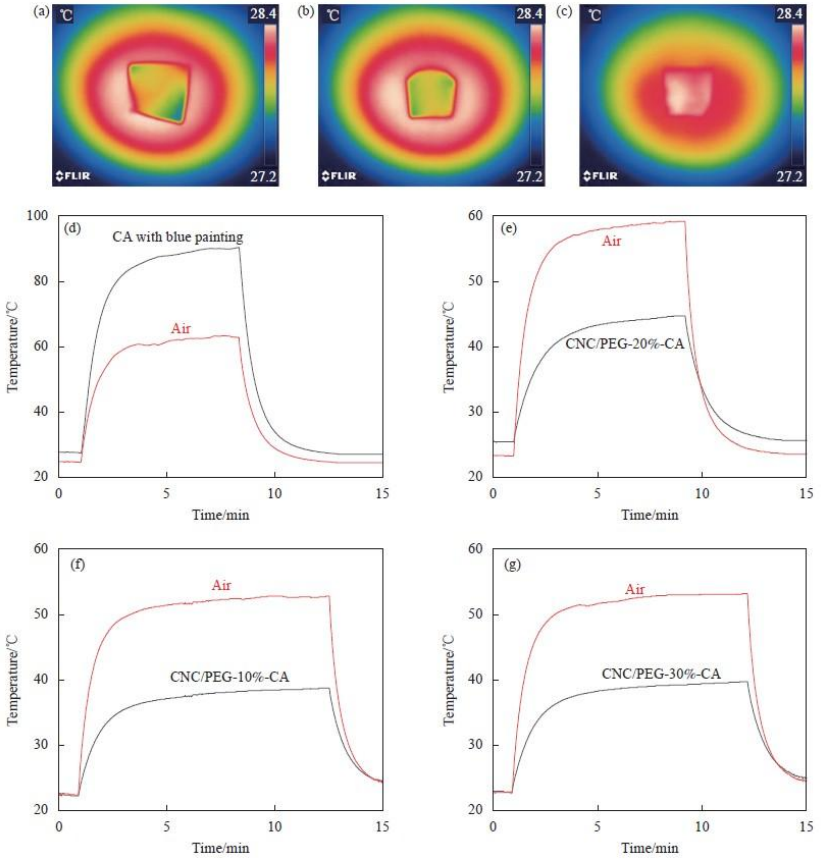

Figure 9 ((a)–(c)) Infrared thermograms of CNC/PEG-20%, CNC/PEG-20%-CA and CA films with blue coatings; Temperature comparison of CA with blue painting and air (d), CNC/PEG-20%-CA and air (e), CNC/PEG-10%-CA and air (f), CNC/PEG-30%-CA and air (g)

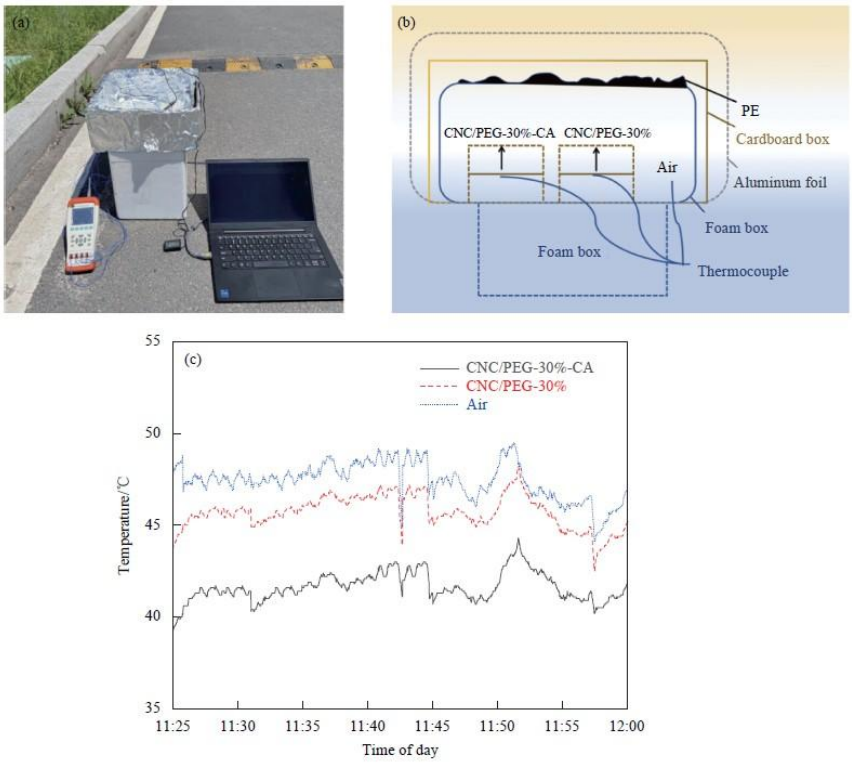

Figure 10 (a), (b) Outdoor testing apparatus for measuring temperatures of CNC/PEG-30%-CA, CNC/PEG-30% and air inside the PE-covered device; (c) Temperature profiles comparison

Figs. 10(a) and 10(b) depict the outdoor testing apparatus for measuring temperatures of CNC/PEG-30%-CA, CNC/PEG-30%, and the air inside the PE-covered device. The entire setup was wrapped in aluminum foil to minimize thermal radiation interference from surrounding buildings. A PE film covered the top to reduce environmental convective and conductive heat transfer. The underlying foam box insulated against ground thermal interference. Thermocouples recorded the temperature within the sample-covered cavity and the air temperature beneath the PE film. Analysis of Fig. 10(c) shows that in an outdoor environment with an average temperature of 25 °C and average humidity of 51%, the composite film achieved an average cooling effect of ~2 °C relative to the air temperature inside the device, while the bilayer composite film achieved an average cooling of ~6 °C.

The radiative cooling performance of the CNC/PEG-CA bilayer composite films originates from the synergistic integration of chiral nematic photonics, polymer chain-mediated structural modulation, and hierarchical porosity-enabled broadband thermal emission, which collectively resolve the long-standing trade-off between structural color tunability and high cooling efficiency in sustainable passive cooling materials. At the nanoscale, the chiral nematic architecture of the CNC/PEG composite layer is preserved via a carefully balanced self-assembly process: acid-hydrolyzed CNCs with a high Zeta potential (−32.2 mV) maintain colloidal stability through strong electrostatic repulsion, enabling the spontaneous formation of a left-handed helical superstructure during slow solvent evaporation. The incorporation of PEG—with a refractive index (1.44) closely matching that of CNC (1.41)—does not disrupt this ordered arrangement but instead acts as a molecular spacer: PEG macromolecules penetrate the interstitial voids between CNC nanorods, inducing a progressive expansion of the helical pitch (P) from 0.30 μm (10 wt% PEG) to 0.46 μm (30 wt% PEG), as confirmed by SEM and polarized optical microscopy (POM). This pitch modulation directly governs structural color via Bragg's law ($\lambda = nP\cos\theta$), where the constant average refractive index (n) and fixed incident angle (θ) ensure that λ redshifts linearly with P, shifting the film's appearance from blue-green to red. Critically, this chiral nematic structure enables selective visible light reflection without absorption: the periodic variation in refractive index across the helical layers generates a high reflectance peak (up to 68.5% in the visible range for CNC/PEG-30%), minimizing solar heat gain while producing vivid, angle-dependent structural colors absent in conventional pigment-based systems.

The bilayer design further amplifies cooling efficiency by combining the photonic functionality of the CNC/PEG layer with the broadband infrared emissivity of the porous CA substrate. In the atmospheric window (8–13 μm), the CNC/PEG layer leverages molecular vibrational modes—specifically O–H stretching (6.9–7.6 μm), C–O bending (7.6–9.5 μm), and C–H deformation (11.1–14.3 μm)—to achieve a peak emissivity of 93.0%, facilitating efficient radiative heat loss to outer space. However, the single-layer film's cooling performance is limited by its moderate solar reflectance (~68.5%). The integration of a porous CA membrane addresses this limitation: the CA layer's interconnected micropores (observed via SEM) act as Mie scattering centers for solar radiation, boosting total solar reflectance to 91.8% across the 0.3–2.5 μm range. Simultaneously, the CA layer's inherent infrared transparency in the atmospheric window allows the underlying CNC/PEG layer to maintain its high emissivity (peaking at 68.0% for the bilayer system), creating a decoupled optical pathway where visible light is reflected by the CA/CNC/PEG interface while thermal radiation escapes through the CA matrix. This synergy is quantitatively validated by indoor xenon lamp tests: the bilayer film achieves a 14.3°C temperature reduction relative to ambient, far exceeding the 3.4°C cooling of the single-layer CNC/PEG film. Outdoor trials further confirm practical efficacy, with the bilayer film maintaining a 6°C sub-ambient temperature under real-world solar irradiance (25°C ambient, 51% humidity). Notably, the system avoids the heat absorption penalty of traditional dyes, as structural color arises from photonic interference rather than molecular absorption, and PEG's hydrophilicity is mitigated by the CA layer's hydrophobicity and the bilayer's structural encapsulation. This multi-scale mechanism—spanning molecular-level pitch control, nanoscale chiral photonics, and microscale porous scattering—establishes the CNC/PEG-CA bilayer as a paradigm for sustainable, colorful radiative cooling.

While the CNC/PEG-CA bilayer composite demonstrates exceptional lab-scale performance, several critical avenues warrant further exploration to advance its practical deployment and expand its utility in real-world applications. First, the current system faces a moisture sensitivity challenge: CNC/PEG-40% films exhibit swelling-induced pitch expansion due to PEG's hygroscopicity, disrupting structural color and cooling performance.

Future work should focus on developing hydrophobic surface treatments—such as silane coupling agents (e.g., octadecyltrimethoxysilane) or bio-based wax coatings—to encapsulate the chiral nematic structure without compromising optical clarity. Alternatively, replacing PEG with less hygroscopic polyols (e.g., polypropylene glycol) or crosslinking PEG via UV-induced thiol-ene reactions could stabilize the helical pitch under humid environments (e.g., tropical climates with >80% relative humidity). Second, the current color gamut is limited to blue-red shifts via pitch modulation; expanding to near-infrared (NIR)-reflective structural colors would further enhance cooling efficiency, as NIR accounts for ~50% of solar irradiance. This could be achieved by incorporating high-refractive-index nanoparticles (e.g., TiO_2, ZnO) into the CNC matrix to increase the refractive index contrast (Δn) between helical layers, enabling Bragg reflection to extend into the NIR region. Third, scalability remains a key bottleneck: the current slow-evaporation method is time-consuming (~2–3 days) and unsuitable for roll-to-roll manufacturing. Exploring rapid drying techniques—such as solvent exchange with volatile alcohols (e.g., ethanol, isopropanol) or convective air drying with controlled humidity—could accelerate film formation while preserving chiral order. Additionally, pilot-scale experiments using blade-coating or slot-die coating on flexible substrates (e.g., polyethylene terephthalate) would validate industrial viability. Fourth, long-term durability testing is essential: accelerated weathering (UV, thermal cycling, mechanical abrasion) and outdoor aging trials (6–12 months) should evaluate color fastness, emissivity retention, and structural integrity. For example, UV-induced degradation of CNC's glycosidic bonds could be mitigated by adding trace amounts of UV stabilizers (e.g., hindered amine light stabilizers) compatible with the bio-based matrix. Fifth, the current bilayer design relies on double-sided tape for adhesion; developing covalent bonding strategies—such as plasma-treated CA surfaces reacting with CNC's hydroxyl groups—would improve interfacial strength and prevent delamination during wind or rain exposure. Sixth, expanding functionality via multifunctional integration could broaden application scenarios: embedding thermochromic pigments into the CA layer could create temperature-indicating cooling films, while incorporating antimicrobial agents (e.g., chitosan nanoparticles) could enable use in food packaging or medical textiles. Seventh, computational modeling (e.g., finite-difference time-domain simulations for photonic bandgap prediction, COMSOL Multiphysics for heat transfer optimization) could accelerate material design by mapping the relationship between CNC aspect ratio, PEG molecular weight, and cooling performance, reducing trial-and-error experimentation. Eighth, environmental and economic assessments are critical for commercial translation: life cycle analysis (LCA) should compare the carbon footprint of CNC/PEG-CA films against conventional cooling materials (e.g., white paints, polymer-based radiative coolers), while techno-economic analysis (TEA) should evaluate raw material costs (CNC extraction efficiency, PEG pricing) and manufacturing energy inputs. Finally, field trials in diverse climates—from arid regions (low humidity, high solar irradiance) to urban heat islands (high pollution, reflective surfaces)—would validate real-world performance and guide application-specific optimizations. By addressing these fundamental and applied research gaps, CNC/PEG-CA bilayers could evolve from a laboratory curiosity to a commercially viable solution for sustainable building envelopes, wearable cooling textiles, and agricultural mulching films, contributing to global efforts to mitigate urban overheating and reduce energy consumption in cooling systems.

3 Conclusion

In this study, cellulose nanocrystals (CNC) and polyethylene glycol (PEG) were blended at varying ratios, and structurally colored composite films with radiative cooling performance were fabricated via self-assembly. These structural color composite films were combined with porous cellulose acetate (CA) films to prepare bilayer composite films possessing both radiative cooling and structural color characteristics. Performance analyses of both film types yielded the following conclusions:

(1) CNC/PEG composite films possess a chiral nematic structure and vivid structural color, exhibiting distinct birefringence. As PEG content increases, the pitch of the chiral nematic structure enlarges, leading to a redshift in the reflection wavelength and subsequent alteration of the film's structural color.

(2) FTIR and UV-vis analyses reveal that the composite film achieves a reflectance of up to 93.0% within the 0.25–2.5 μm wavelength range, while the bilayer composite film reaches 68.0%. The composite film exhibits an emissivity of up to 68.5% in the "atmospheric window" (8–13 μm), whereas the bilayer composite film achieves an emissivity of up to 91.8%.

(3) Under xenon lamp irradiation, CNC/PEG structural color composite films demonstrate radiative cooling performance, averaging a temperature reduction of approximately 3.4 °C compared to the internal air temperature. Integration with porous CA film significantly enhances cooling performance, with the bilayer film averaging a reduction of approximately 14.3 °C. Outdoor tests confirm cooling effects of approximately 2 °C for the composite film and approximately 6 °C for the bilayer composite film relative to ambient temperature.

References

[1] SHU Z K, LI W X, ZHANG J Y, et al. Historical changes and future trends of extreme precipitation and high t emperature in China[J]. Strategic Study of CAE, 2022, 24(5): 116-125
[2] ZUO Z Y, XIAO D, HE Q. Role of the warming trend in global land surface air temperature variations[J]. Sci China Earth Sci, 2021, 51(6): 941-946
[3] FIXSEN D J, KOGUT A, LEVIN S, et al. The temperature of the cosmic microwave background at 10 GHz[J]. Astrophys J, 2004, 612(1): 86.
[4] MUNDAY J N. Tackling climate change through radiative cooling[J]. Joule, 2019, 3(9): 2057-2060.
[5] CARLOSENA L, RUIZ-PARDO A, RODRÍGUEZ-JARA E A, et al. Worldwide potential of emissive materials bas ed radiative cooling technologies to mitigate urban overheating[J]. Build Environ, 2021, 243: 110694.
[6] TAO S, WAN Q, XU Y, et al. Incorporation form-stable phase change material with passive radiative coolin g emitter for thermal regulation[J]. Energy Build, 2021, 288: 113031.
[7] YIN X, YANG R, TAN G, et al. Terrestrial radiative cooling: Using the cold universe as a renewable and susta inable energy source[J]. Science, 2020, 370(6518): 786-791.
[8] BIJARNIYA J P, SARKAR J, MAITI P. Review on passive daytime radiative cooling: Fundamentals, recent res earches, challenges and opportunities[J]. Renew Sustain Energy Rev, 2020, 133: 110263.
[9] SUN H, HOU C, JI T, et al. Processing bulk wood into a lightweight permeable passive radiative cooling mat erial for energy-efficient building[J]. Compos Part B, 2021, 250: 110426.
[10] XIA G, ZHOU T, ZHANG Y, et al. Operating characteristics analysis and optimization of loop heat pipe radia tion cooling system in space reactor[J]. Nucl Eng Des, 2022, 420: 113043.
[11] CHEN Y, MANDAL J, LI W, et al. Colored and paintable bilayer coatings with high solar-infrared reflectance for efficient cooling[J]. Sci Adv, 2020, 6(17): eaaz5413.
[12] WANG C X, DENG F F, ZOU H, et al. Investigating transparent radiative film for greenhouse cooling[J]. J Ref rig, 2022, 45(1): 63-69
[13] ZHOU L, RADA J, ZHANG H, et al. Sustainable and inexpensive polydimethylsiloxane sponges for daytime r adiative cooling[J]. Adv Sci, 2021, 8(23): 2102502.
[14] ZHU W, DROGUET B, SHEN Q, et al. Structurally colored radiative cooling cellulosic films[J]. Adv Sci, 2022, 9(26): 2202061.
[15] CAI C Y, DING C X, WU X D, et al. Research progress of biomass cellulose based daytime radiative cooling materials[J]. Acta Mater Compos Sin, 2022, 41(11): 5800-5811
[16] SHI T T, LIU D Q, CHENG H F. Research progress of personal thermal management materials based on infr ared radiation regulation[J]. Acta Mater Compos Sin, 2021, 40(5): 2480-2494 [17] BENMOUSSA Y, EZZIANI M, DJIRE A F, et al. Simulation of an energy-efficient cool roof with cellulose-based daytime radiative cool ing material[J]. Mater Today Proc, 2021, 72: 3632-3637.
[17] ANUSUYADEVI P R, SINGHA S, BANERJEE D, et al. Synthetic plant cuticle coating as a biomimetic moisture barrier membrane for structurally colored cellulose films[J]. Adv Mater Interfaces, 2021, 10(7): 2202112.
[18] KIM H H, IM E, LEE S. Colloidal photonic assemblies for colorful radiative cooling[J]. Langmuir, 2020, 36(2 3): 6589-6596.
[19] AN B, XU M C, MA C H, et al. Tuning and application of structural color of cellulose nanocrystals chiral com posite materials[J]. Acta Polym Sin, 2022, 53(3): 211-226
[20] HABIBI Y, LUCIA L A, ROJAS O J. Cellulose nanocrystals: Chemistry, self-assembly, and applications[J]. Che m Rev, 2010, 110(6): 3479-3500.
[21] CUI W B, LIANG T T, WANG Y B, et al. Study of photocatalytic reduction of Cr(VI) by mesoporous titanium dioxide using lignocellulose as template[J]. For Eng, 2021, 39(6): 101-108
[22] ZHANG X J, MA X J. Effects of NaOH concentration on structure and properties of nano-Fe_3O_4/cellulose co mposite membrane[J]. Biomass Chem Eng, 2016, 50(5): 1-6

[23] DAI L L, LI W, CAO J, et al. Preparation and characterization of humidity-sensitive chiral nematic films from nanocrystalline cellulose via evaporation-induced self-assembly method[J]. Polym Mater Sci Eng, 2016, 32(8): 115-119

[24] HUANG Y, CHEN G, LIANG Q, et al. Multifunctional cellulose nanocrystal structural colored film with good flexibility and water-resistance[J]. Int J Biol Macromol, 2020, 149: 819-825.

[25] SHANKER R, RAVI ANUSUYADEVI P, GAMAGE S, et al. Structurally colored cellulose nanocrystal films as trans-reflective radiative coolers[J]. ACS Nano, 2022, 16(7): 10156-10162.